analytical chemistry

pubs.acs.org/ac Article

Screening T-Cell Activity via a Photodetachable DNA-Copolymer Nanocage and Its Therapeutic Application

Yanyun Fang, Yawei Yan, Shiyi Bi, Yingfei Wang, Yue Chen, Peipei Xu,* Huangxian Ju, and Ying Liu*

Cite This: *Anal. Chem.* 2022, 94, 13205−13214 Read Online

ACCESS | Metrics & More | Article Recommendations | Supporting Information

ABSTRACT: Screening T-cell activity and selecting active ones from large *ex vivo*-expanded populations before reinfusion is important for the success of T-cell therapy. Cytokine secretion is the evaluation criterion of cell immune activity. Cell membrane-anchored probes and microchamber-based techniques have been used to screen cytokine secretion at the single-cell level. However, they are either easily affected by nearby cells' secretion or lack of single-cell encapsulation efficiency. Here, we design a photodetachable DNA-copolymer nanocage on the cell membrane for screening the activities of *ex vivo*-expanded T cells by in-situ monitoring cytokine interferon-gamma (IFN-γ) secretion. The ones with good immune activity are selected for therapeutic application. DNA-copolymer nanocage is self-assembled on a cell membrane to encapsulate a single T cell. A self-quenched IFN-γ recognition aptamer is contained in the DNA-copolymer nanocage, which recovers fluorescence in response to IFN-γ secretion to indicate individual T-cell activity. The active T cells are collected after fluorescence-activated cell sorting, irradiated with 5 min UV light to detach nanocage from the cell membrane, and continuously cocultured with downstream cells. The selected Jurkat cells and CD19 CAR-T cells showed improved capabilities for downstream cell activation and cancer cell killing. The cell membrane-detachable DNA-copolymer nanocage-based T-cell activity screening and selection would have promising applications in T-cell therapy.

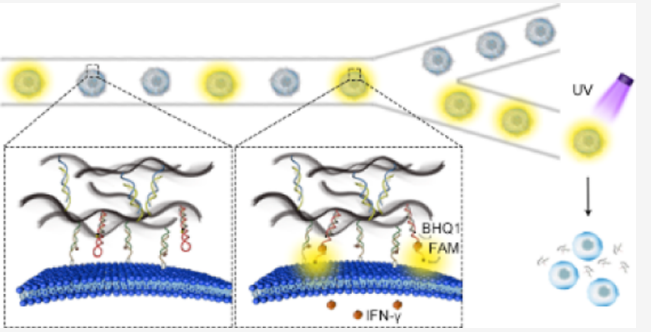

Adoptive cell therapy (ACT) has emerged as a promising therapy for cancer treatment.[1,2] It requires *ex vivo* expansion of immune cells with subsequent reinfusion to the host.[3,4] A large number of T cells with highly heterogeneous composition are generated during *ex vivo* expansion. Some are active and specific to cancer cells, while others are inactive and incapable of recognizing and killing cancer cells.[5] Therefore, real-time screening of their activity with a selection of the active ones for host reinfusion is of great importance to improve T-cell performance *in vivo*.[6]

Cytokines, the cell-secreted proteins, play critical roles in activating immune cells and regulating cell functions.[7−9] To perform quality control (QC) testing of *in vitro*-expanded lymphocytes, the activity of the as-obtained cells is determined by detecting cytokine secretion.[10,11] Many analytical methods, such as the enzyme-linked immunosorbent assay (ELISA),[12] protein electrophoresis,[13] and mass spectrometry[14] have been developed to measure cytokine secretion levels from cell culture media for *in vitro*-expanded cell populations. However, the population-averaged measurement in bulk analysis masks the vast heterogeneity in single-cell secretion capability.[15] Therefore, approaches to monitor cytokine secretion with the single-cell resolution are in urgent need for cell activity screening and selection.

Microchamber formats have been successfully applied for single-cell isolation and corresponding cytokine secretion detections.[16−18] However, the single-cell encapsulation percentage and screening efficiency are low due to Poisson distribution.[15] As the natural boundary to isolate cells from the outside environment,[19,20] the cell membrane has been covalently functionalized with capture antibodies and combined with an immunoassay to distinguish cytokine-secreting cells via fluorescence-activated cell sorting (FACS).[21,22] However, the "open" detection environment of the cell membrane allows the outward diffusion of secreted cytokine, and the interference from nearby cells' secretions also impairs single-cell distinguishing efficiency. The end-point detection manner further covers cytokine secretion dynamics information.[23,24]

Using DNA strands as building blocks, nanostructures have been constructed on the cell membrane to control cell−cell

Received: June 27, 2022
Accepted: September 1, 2022
Published: September 12, 2022

https://doi.org/10.1021/acs.analchem.2c02763
Anal. Chem. 2022, 94, 13205−13214

Scheme 1. Schematic Illustration of DNA-Copolymer Nanocage-Encapsulated T Cells for Activity Sorting; (A) Construction of Detachable DNA-Copolymer Nanocage on the Cell Membrane; (B) Its Application in Single-Cell IFN-γ Secretion Detection for T-Cell Activity Screening and Selection with Subsequent Detachment from the Cell Membrane for Therapeutic Usage (C)

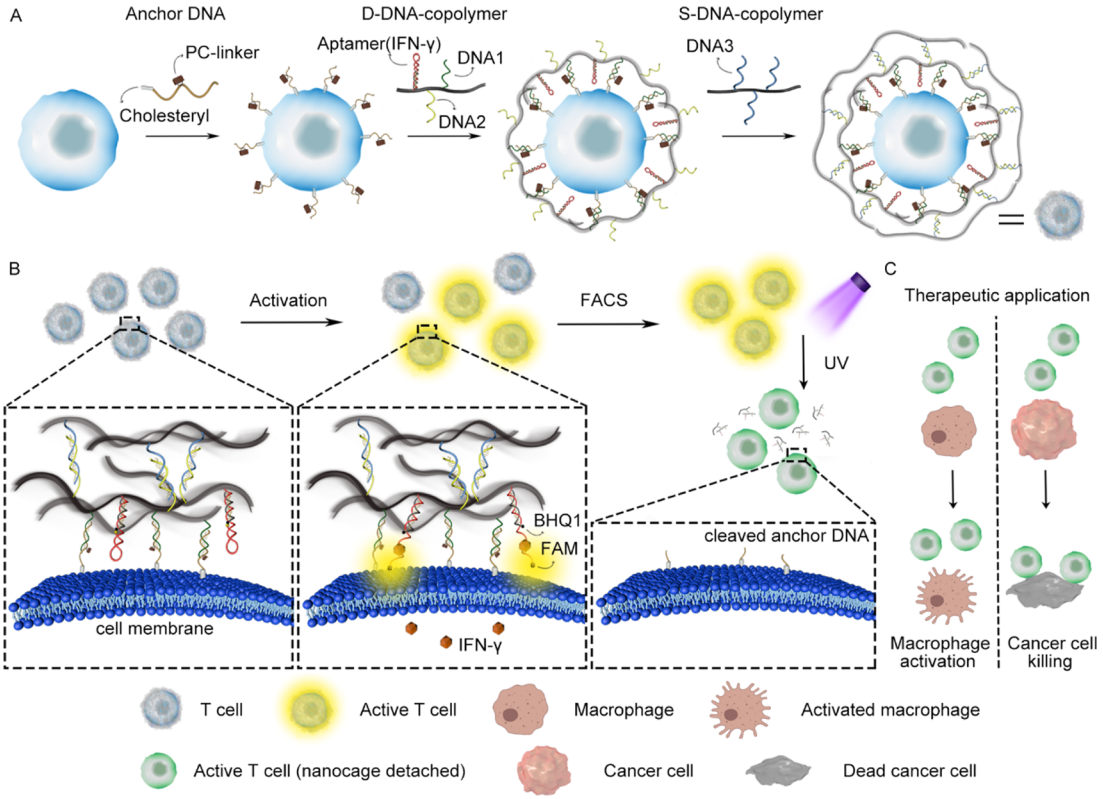

interaction.[25] However, due to the lack of cell membrane wrapping density and the incapability of reversible modification, they have not been used for single-cell activity screening and selection up to now. Here, we develop a detachable DNA-copolymer nanocage on the cell membrane of *ex vivo*-expanded T cells to screen cell activity, and the selected active T cells demonstrate improved performance in therapeutic application. Anchor DNA is functionalized with cholesteryl and photocleavable linker (PC-linker) containing an *o*-nitrobenzyl functional group that can be activated upon UV irradiation and cleaves anchor DNA. Anchor DNA was inserted into the T-cell membrane via hydrophobic−hydrophobic interaction and detached from the cell membrane with UV exposure. The detection DNA-copolymer (D-DNA-copolymer) and sealing DNA-copolymer (S-DNA-copolymer) are synthesized via copolymerization of acrylamide and acrydite-modified DNA strands. The D-DNA-copolymer contains DNA1 that hybridizes with anchor DNA, an aptamer for cytokine interferon-γ [aptamer (IFN-γ)] that specifically recognizes IFN-γ, and DNA2. S-DNA-copolymer contains DNA3 that hybridizes with DNA2. The anchor DNA-functionalized cell is successively hybridized with the D-DNA-copolymer and S-DNA-copolymer to construct the detachable DNA-copolymer nanocage on the cell membrane (Scheme 1A). IFN-γ, a proinflammatory cytokine, which is typically used in the cytokine release assay for cell immune activity characterization, is chosen as the model detection target. Aptamer (IFN-γ) has a self-quenched hairpin structure with fluorescein (FAM) and a corresponding quencher black hole quencher labeled at adjacent positions. The hairpin structure unfolds upon IFN-γ recognition and results in FAM fluorescence recovery on the DNA-copolymer nanocage to indicate activated T cells. The cell activity is screened via FACS, and the selected active T cells are subsequently exposed to UV light to cleave the PC-linker and detach the DNA-copolymer nanocage from the cell membrane (Scheme 1B). The detachable DNA-copolymer nanocage shows a successful selection of active T cells from *ex vivo*-expanded populations. The selected active T cells demonstrate enhanced immune functions in downstream cell activation and cancer cell killing (Scheme 1C). The as-presented T-cell immune activity sorting strategy based on the cell membrane-detachable DNA-copolymer nanocage would have a promising contribution to ACT.

EXPERIMENTAL SECTION

Synthesis of DNA-Copolymers. Acrylamide/acrydite-DNA-copolymers were synthesized by copolymerizing acrylamide and acrydite-functionalized DNA strands. To prepare the detection DNA-copolymer (D-DNA-copolymer), 150 μL of a solution containing DNA1 (10 μM), DNA2 (30 μM), and aptamer (IFN-γ) (10 μM) were mixed with 30 μL of 2% acrylamide, 10 μL of initiator 10% APS, and 10 μL of the accelerator tetramethylethylenediamine (TEMED) in Tris buffer (10 mM Tris, 50 mM NaCl, 10 mM $MgCl_2$, pH 8.0). The mixture solution was polymerized by incubating at room temperature for 5 min and subsequently at 4 °C for 24 h. The resulting D-DNA-copolymer was purified from unreacted monomer units, salts, and initiators with a Microcon (Millipore) spin filter unit (MWCO 30 kD). The sealing DNA-copolymer (S-DNA-copolymer) was synthesized by mixing 150 μL of DNA3 (30 μM) with 30 μL of 2% acrylamide, 10 μL of initiator 10% APS, and 10 μL of the

https://doi.org/10.1021/acs.analchem.2c02763
Anal. Chem. 2022, 94, 13205−13214

accelerator TEMED in Tris buffer (10 mM Tris, 50 mM NaCl, 10 mM $MgCl_2$, pH 8.0), polymerized, and purified according to the similar procedure as the D-DNA-copolymer. The as-obtained DNA-copolymers were dissolved in 200 μL of water for future use.

Cell Culture. U937 cells (Keygen Biotech, China) and Jurkat cells (CoBioRes Biosciences, China) were cultured in RPMI-1640 medium containing 10% FBS, penicillin (100 U/mL), and streptomycin (100 μg/mL). RAW264.7 cells (Keygen Biotech, China) and 4T1 cells (Keygen Biotech, China) were cultured in Dulbecco's modified Eagle's medium containing 10% FBS, penicillin (100 U/mL), and streptomycin (100 μg/mL). Raji cells were kindly provided by Nanjing Biotech and Pharmaceutical Valley (China), and CD19 CAR-T cells were kindly provided by Nanjing Drum Tower Hospital. The usage of CAR-T cells was approved by the Ethics Committee of Nanjing Drum Tower Hospital with the study number 2018-144-02. All cell lines were maintained at 37 °C under a humidified 5% CO_2 atmosphere. The cell numbers were counted using a Countess II automated cell counter (Invitrogen, USA).

Construction of the DNA-Copolymer Nanocage on Cell Membranes. The D-DNA-copolymer and S-DNA-copolymer were successively hybridized to the U937 cell to verify the construction of the DNA-copolymer nanocage on the cell membrane. U937 cells were incubated with different concentrations of anchor DNA (200, 500, 1000, and 2000 nM) at 37 °C to optimize the construction efficiency of the DNA-copolymer nanocage. After washing them with 1×PBS three times, the cells were imaged by confocal laser scanning microscopy (CLSM), and the fluorescence intensity was collected from 560 to 600 nm under a 543 nm excitation. 1000 nM anchor DNA was chosen as the optimal anchoring condition.

To assemble the DNA-copolymer nanocage on the cell membrane, anchor DNA-immobilized U937 cells were sequentially incubated with the D-DNA-copolymer (1 μM) and tetramethylrhodamine (TAMRA)-labeled S-DNA-copolymer (1 μM) at 37 °C for 5 min, respectively. After being washed with 1×PBS three times, the cells were imaged by CLSM. For the colocalization experiment, the cells were stained with DiO (5 μM) for 5 min before imaging. The DiO fluorescence was collected from 500 to 540 nm under a 488 nm excitation. The TAMRA fluorescence of the as-obtained DNA-copolymer was collected from 560 to 600 nm under 543 nm excitation. Z-stacked images were collected to demonstrate the integral wrapping of the DNA-copolymer nanocage on the cell membrane. Control experiments were performed using the D-DNA-copolymer with mismatched DNA1, D-DNA-copolymer in the absence of DNA2, and S-DNA-copolymer with mismatched DNA3.

To verify the detachment of the DNA-copolymer nanocage from the U937 cell membrane, TAMRA was used to label the DNA-copolymer. The U937 cell was assembled with the TAMRA-labeled DNA-copolymer, exposed to 5 min UV irradiation, and imaged using CLSM after rinsing with PBS.

The internalization of the DNA-copolymer was verified by incubating U937 cells (encapsulated with TAMRA-labeled DNA-copolymer) in 1×PBS at 37 °C for 15 min and imaged with CLSM. The cholesteryl-functionalized aptamer (IFN-γ) (TAMRA-labeled) was treated under the same reaction condition and imaged by CLSM.

Real-Time Detection of IFN-γ Secretion via the Cell Membrane-Constructed DNA-Copolymer Nanocage. The feasibility of the cell membrane-constructed DNA-copolymer nanocage for IFN-γ detection was verified by incubating the DNA-copolymer nanocage-encapsulated U937 cells in fresh RPMI-1640 media containing recombinant IFN-γ (40, 200, and 400 nM) for 30 min at 37 °C. FAM fluorescence recovery from the DNA-copolymer nanocage was collected. To detect cellular secretion of IFN-γ in real time, DNA-copolymer nanocage-encapsulated Jurkat cells were cultured in fresh RPMI-1640 media containing phorbol 12-myristate-13-acetate (PMA) (50 ng/mL) and ionomycin (1 μg/mL), and the FAM fluorescence recovery from the DNA-copolymer nanocage was measured according to time. The TAMRA-labeled DNA-copolymer nanocage was used for the colocalization experiment. FAM fluorescence was collected from 500 to 540 nm under 488 nm excitation, and TAMRA fluorescence was collected from 560 to 600 nm under 543 nm excitation.

T-Cell-Macrophage Cell Communication and Verification of Downstream Cell Activation. The DNA-copolymer nanocage-encapsulated Jurkat cells were cultured in fresh RPMI-1640 medium containing PMA (50 ng/mL) and ionomycin (1 μg/mL) to stimulate IFN-γ secretion. The cells were sorted via FACS according to FAM fluorescence recovery at 10 min after stimulation. The cells with higher FAM fluorescence recovery were selected and exposed to UV irradiation for 5 min to detach the DNA-copolymer nanocage from the cell membrane. The selected Jurkat cells were cocultured with macrophage RAW264.7 cells in a Transwell chamber for 24 h. To evaluate the activation of downstream RAW264.7 cells, their capability of cytokine TNF-α secretion was measured from the supernatant of the coculture medium. In addition, the cell killing capability of RAW264.7 cells was evaluated by coculturing them with 4T1 cells at a ratio of 2:1 for 24 h, and the viability of 4T1 cells was measured subsequently. Control experiments were performed by coculturing RAW264.7 cells with unselected Jurkat cells, and TNF-α secretion capability and 4T1 cell killing capability were evaluated according to the same procedures above.

CD19 CAR-T Cell Activation, Selection, and Killing Effect Evaluation. CD19 CAR-T cells were coincubated with eFluor 670-stained Raji cells at a ratio of 2:1 for 2 h. The cell mixture was assembled with the DNA-copolymer nanocage on the cell membrane, and CD19 CAR-T-cell activation was evaluated via IFN-γ secretion by measuring FAM fluorescence recovery from 500 to 540 nm under 488 nm excitation. TAMRA was also labeled on the DNA-copolymer nanocage to indicate its location on the cell membrane, and TAMRA fluorescence was recorded from 560 to 600 nm under 543 nm excitation. CD19 CAR-T cells coculturing with Jurkat cells were set as a negative control to verify the activation of CD19 CAR-T cells.

CD19 CAR-T cells that demonstrated good IFN-γ secretion capability were sorted by FACS, and the selected cells were exposed to UV light for 5 min to detach the DNA-copolymer nanocage from the cell membrane. Subsequently, these selected CD19 CAR-T cells were cocultured with Raji cells for 8 h, and their killing capability was evaluated by measuring Raji cell viability using a CCK-8 kit. To perform a control experiment to demonstrate the contribution of CD19 CAR-T-cell screening to its killing effect, eFluor 670-stained Raji cells were sorted via FACS and discarded from the CD19 CAR-T cells and Raji cell coculture. All the CD19 CAR-T cells were

https://doi.org/10.1021/acs.analchem.2c02763
Anal. Chem. 2022, 94, 13205−13214

kept and cocultured with Raji cells with subsequent Raji cell viability measurement.

RESULTS AND DISCUSSION

Preparation of the Detachable DNA-Copolymer Nanocage. The D-DNA-copolymer was synthesized with acrylamide, acrydite-functionalized DNA strands, DNA1, aptamer (IFN-γ), and DNA2. The S-DNA-copolymer was synthesized with acrylamide and acrydite-functionalized DNA3. The successful copolymerizations were confirmed by PAGE analysis. DNA1, DNA2, and DNA3 showed a clear single band with high mobility, respectively, while the bands for the D-DNA-copolymer and S-DNA-copolymer demonstrated much lower mobilities (Figure S1). To further verify the synthesis of the DNA-copolymer, the dye FAM was modified on DNA1 (DNA1-FAM) to trace its location during the copolymerization process. After the copolymerization reaction of acrylamide and DNA1-FAM, the reaction mixture was purified by the spin filter, which retained the DNA-copolymer in concentrate and removed unreacted DNA1-FAM in the filter. There was obvious FAM fluorescence displayed in the concentrate with little fluorescence in the filtrate (Figure S2A), indicating that DNA1-FAM was retained in the as-obtained DNA-copolymer. On the contrary, naDNA1-FAM in the absence of the acrydite functional group only showed FAM fluorescence in the filtrate (Figure S2B).

The hybridization specificities of anchor DNA with DNA1 and DNA2 with DNA3 were verified via PAGE analysis, which showed a new single band with lower mobility both for the mixture of anchor DNA and DNA1, and the mixture of DNA2 and DNA3 (Figure S3, lane 5,6). On the contrary, the mixture of anchor DNA and DNA2 and the mixture of DNA1 and DNA3 showed separate bands (Figure S3, lane 7,8). The specific hybridization of DNA strands guaranteed the successful construction of the DNA-copolymer nanocage. The *in vitro* hybridizations of anchor DNA with the D-DNA-copolymer and D-DNA-copolymer with the S-DNA-copolymer were further verified via specific fluorescence quenching. DNA1-FAM and Cy3-labeled DNA2 (DNA2-Cy3) were used separately to synthesize two kinds of fluorescent D-DNA-copolymers: D-DNA-copolymer-FAM_{DNA1} and D-DNA-copolymer-$Cy3_{DNA2}$. BHQ1 was labeled on anchor DNA (anchor DNA-BHQ1), which substantially decreased FAM fluorescence when the formed anchor DNA-DNA1 duplex with BHQ1 and FAM were located at proximate positions in the duplex (Figure 1A,B). S-DNA-copolymer-$BHQ2_{DNA3}$ was synthesized with DNA3-BHQ2, and the hybridization of S-DNA-copolymer-$BHQ2_{DNA3}$ with D-DNA-copolymer-$Cy3_{DNA2}$ strongly decreased Cy3 fluorescence due to the proximate locations of Cy3 and BHQ2 in the DNA2−DNA3 duplex (Figure 1A,C). These results indicated conjugation with the polymer did not affect the hybridization efficiencies of DNA strands. On the contrary, incubating D-DNA-copolymer-FAM_{DNA1} with mismatched anchor DNA-BHQ1 (m-anchor DNA-BHQ1) or incubating D-DNA-copolymer-$Cy3_{DNA2}$ with ns-S-DNA-copolymer-$BHQ2_{DNA3'}$ (DNA3′ has mismatched sequence with DNA2) barely decreased FAM or Cy3 fluorescence, excluding the possibility of fluorescence decrease due to polymer twining (Figure 1B,C). DAPI, a dye inserted into the base pair of DNA duplex, was incubated with the mixture of D-DNA-copolymer and S-DNA-copolymer and displayed obvious fluorescence. Only incubating DAPI with the D-DNA-copolymer, S-DNA-copolymer, or the mixture of

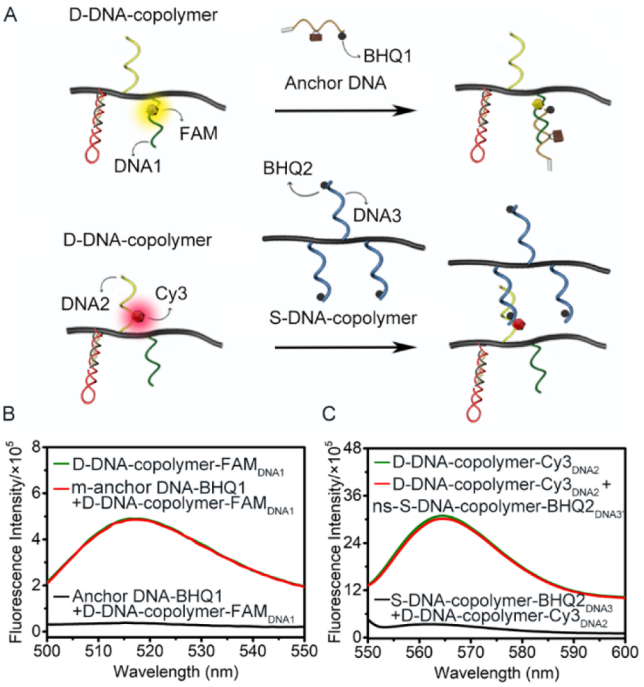

Figure 1. Characterizations of the DNA-copolymer nanocage. (A) Schematic illustrations and fluorescence spectra of (B) D-DNA-copolymer-FAM_{DNA1} hybridizing with anchor DNA-BHQ1 and (C) D-DNA-copolymer-$Cy3_{DNA2}$ hybridizing with S-DNA-copolymer-$BHQ2_{DNA3}$.

D-DNA-copolymer and ns-S-DNA-copolymer$_{DNA3'}$ showed very limited fluorescence (Figure S4). These results confirmed the formation of DNA-copolymer nanocages *in vitro*.

Construction of Detachable DNA-Copolymer Nanocages on the Cell Membrane. Cholesteryl-functionalized anchor DNA was inserted into the cell membrane via hydrophobic−hydrophobic interaction to enable the subsequent assembly of the D-DNA-copolymer and S-DNA-copolymer. The efficient immobilization of anchor DNA on the cell membrane was verified by incubating the model cell U937 with FAM-labeled anchor DNA (anchor DNA−FAM). It demonstrated clear FAM fluorescence around the cell membrane, which overlapped well with that of membrane dye DiD (Figure 2A). The effective insertion of anchor DNA in the cell membrane was also confirmed by flow cytometry, which showed obvious FAM fluorescence for anchor DNA−FAM-incubated U937 cells, while negligible fluorescence was observed from cholesteryl-free anchor DNA−FAM (cf-anchor DNA−FAM)-incubated U937 cells (Figure S5), excluding the possibility of anchor DNA nonspecific adsorption on the cell membrane. The sequential assembly of the D-DNA-copolymer and S-DNA-copolymer on the cell membrane was verified by CLSM. D-DNA-copolymer-FAM_{DNA1} showed clear FAM fluorescence at the anchor DNA-functionalized U937 cell membrane (Figure S6A). Little FAM fluorescence was observed when incubating D-DNA-copolymer-FAM_{DNA1} with bare U937 cells in the absence of anchor DNA functionalization (Figure S6B) or incubating anchor DNA-functionalized U937 cells with ns-D-DNA-copolymer-$FAM_{DNA1'}$ (DNA1′ has mismatched sequence with anchor DNA) (Figure S6C). D-DNA-copolymer-FAM_{DNA1} and S-DNA-copolymer-$TAMRA_{DNA3}$ coencapsulated U937 cells demonstrated a good overlap of TAMRA fluorescence with FAM fluorescence

https://doi.org/10.1021/acs.analchem.2c02763
Anal. Chem. 2022, 94, 13205−13214

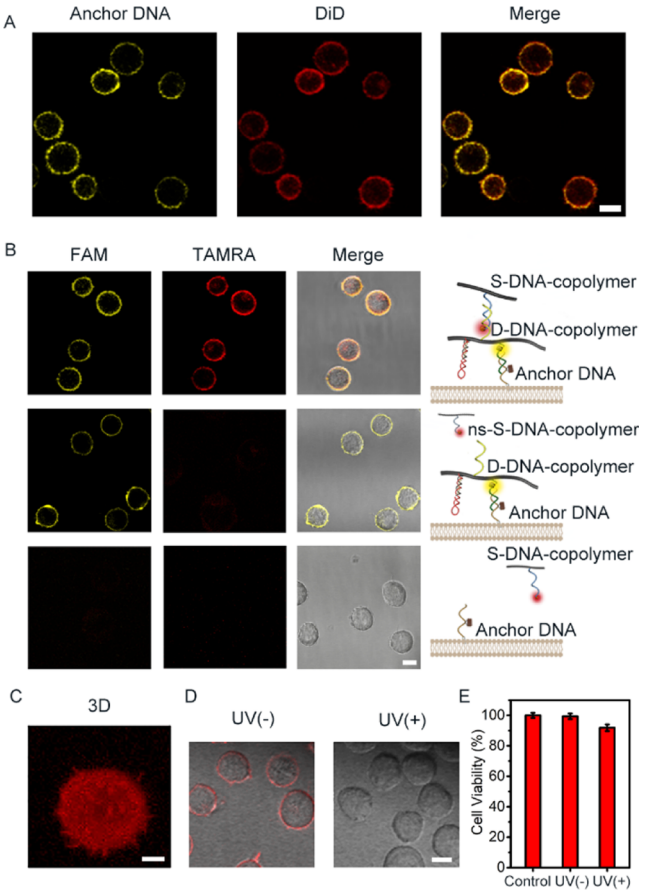

Figure 2. Construction of the detachable DNA-copolymer nanocage on the cell membrane. (A) Confocal fluorescence microscopic images of U937 cells treated with anchor DNA−FAM and DiD. The scale bar is 10 μm. (B) CLSM images of anchor DNA-modified U937 cells incubated with D-DNA-copolymer-FAM_{DNA1} + S-DNA-copolymer-$TAMRA_{DNA3}$ (top line), D-DNA-copolymer-FAM_{DNA1} and ns-S-DNA-copolymer-$TAMRA_{DNA3'}$ (middle line), and only S-DNA-copolymer-$TAMRA_{DNA3}$ (bottom line). The scale bar is 10 μm. (C) 3D-stack image of the DNA-copolymer-encapsulated cell. The scale bar is 5 μm. (D) CLSM images of the TAMRA-labeled DNA-copolymer nanocage-encapsulated U937 cells before [UV(−)] and after 5 min of UV irradiation [UV(+)] with (E) corresponding cell viability results. Control indicates untreated U937 cells. The scale bar in (D) is 10 μm. The error bars in (E) indicate means ± S.D. (n = 3).

(Figure 2B, top line), as well as TAMRA fluorescence with the cell membrane dye DiO (Figure S7), indicating the successful construction of the DNA-copolymer nanocage on the U937 cell membrane. On the contrary, little TAMRA fluorescence was observed when incubating ns-S-DNA-copolymer-$TAMRA_{DNA3'}$ (mismatched DNA3 sequence) with D-DNA-copolymer-FAM_{DNA1} preassembled U937 cells (Figure 2B, middle line) or incubating anchor DNA-immobilized U937 cells with S-DNA-copolymer-$TAMRA_{DNA3}$ in the absence of D-DNA-copolymer-FAM_{DNA1} (Figure 2B, bottom line). The successful construction of the DNA-copolymer nanocage on the cell membrane was further confirmed by flow cytometry. D-DNA-copolymer-FAM_{DNA1} only showed FAM fluorescence on anchor DNA-immobilized U937 cells (Figure S8A). In addition, S-DNA-copolymer-FAM_{DNA3} only showed FAM fluorescence on the U937 cell membrane that was preassembled with the D-DNA-copolymer (Figure S8B). The concentration of anchor DNA was optimized for the construction of the DNA-copolymer nanocage and achieved saturated TAMRA fluorescence from S-DNA-copolymer-$TAMRA_{DNA3}$ on the cell membrane at 1 μM, indicating the sufficient encapsulation of the DNA-copolymer nanocage on U937 cells (Figure S9). Integrating image slices into 3D reconstruction showed the entire coating of the DNA-copolymer nanocage on the cell membrane (Figures 2C and S10). Scanning electron microscopy images also demonstrated a smoother surface morphology for DNA-copolymer-nanocage-encapsulated U937 cells (Figure S11). Anchor DNA was modified with a PC-linker for controllable detachment of the DNA-copolymer nanocage (Figure S12A). UV light irradiation-cleaved anchor DNA and showed the appearance of a shorter DNA strand with higher mobility on polyacrylamide gel electrophoresis (PAGE) (Figure S12B). TAMRA-labeled DNA-copolymer nanocage-encapsulated U937 cells were further used to demonstrate the controllable detachment of the nanocage, which barely showed TAMRA fluorescence from the cell membrane upon 5 min of UV exposure (Figure 2D). This result indicated the smooth and complete removal of the DNA-copolymer nanocage from the cell membrane. The construction and detachment of the DNA-copolymer nanocage from the cell membrane showed little effect on cell viability measured by the CCK-8 kit (Figure 2E).

Detection of IFN-γ Secretion from the Single T Cell. IFN-γ is a proinflammatory cytokine produced by immune cells upon antigen stimulation. Measuring IFN-γ secretion is a standard approach to evaluate immune cell activity.[26,27] The aptamer (IFN-γ), a self-quenching duplex DNA strand, was designed to monitor IFN-γ secretion in real time. The aptamer (IFN-γ) was composed of a FAM-labeled hairpin-structured aptamer that specifically recognized IFN-γ and a complementary BHQ1-labeled DNA quenching strand. BHQ1 was located in proximity to FAM to quench its fluorescence in its original state. IFN-γ binding changed the structure of the hairpin aptamer and pulled FAM away from BHQ1, instantly resulting in fluorescence recovery (Figure 3A).

The direct fluorescence recovery upon target recognition endowed the DNA-copolymer nanocage with the capability of IFN-γ secretion monitoring. To verify the sensing capability of aptamer (IFN-γ), it was challenged with different concentrations of recombinant IFN-γ and demonstrated gradual fluorescence increase (Figure 3B). FAM fluorescence recovery was barely observed when challenging the aptamer (IFN-γ) with PBS and BSA, or challenging a nonspecific aptamer (IFN-γ) [ns-aptamer (IFN-γ)] with IFN-γ (Figure S13A). TAMRA was labeled on the aptamer (IFN-γ) to indicate its location, which showed clear and even TAMRA fluorescence on the entire cell membrane of U937 cells (Figure 3C). This indicated the sufficient and uniform distribution of the aptamer (IFN-γ) in the DNA-copolymer nanocage, which contributed to the fast and accurate response of IFN-γ secretion. To verify the IFN-γ sensing capability of the DNA-copolymer nanocage, U937 cells, which are incapable of IFN-γ secretion, were assembled with the DNA-copolymer nanocage and challenged with different concentrations of recombinant IFN-γ. It demonstrated gradually increased intensity of FAM fluorescence recovery upon IFN-γ concentration (Figure 3D,E). A sensing specificity experiment was also conducted on DNA-copolymer nanocage-encapsulated U937 cells, which only showed FAM fluorescence recovery in response to IFN-γ (Figure S13B). Copolymerization with acrylamide contributed to the stability of the aptamer (IFN-γ)-TAMRA on the cell membrane, which

https://doi.org/10.1021/acs.analchem.2c02763
Anal. Chem. 2022, 94, 13205−13214

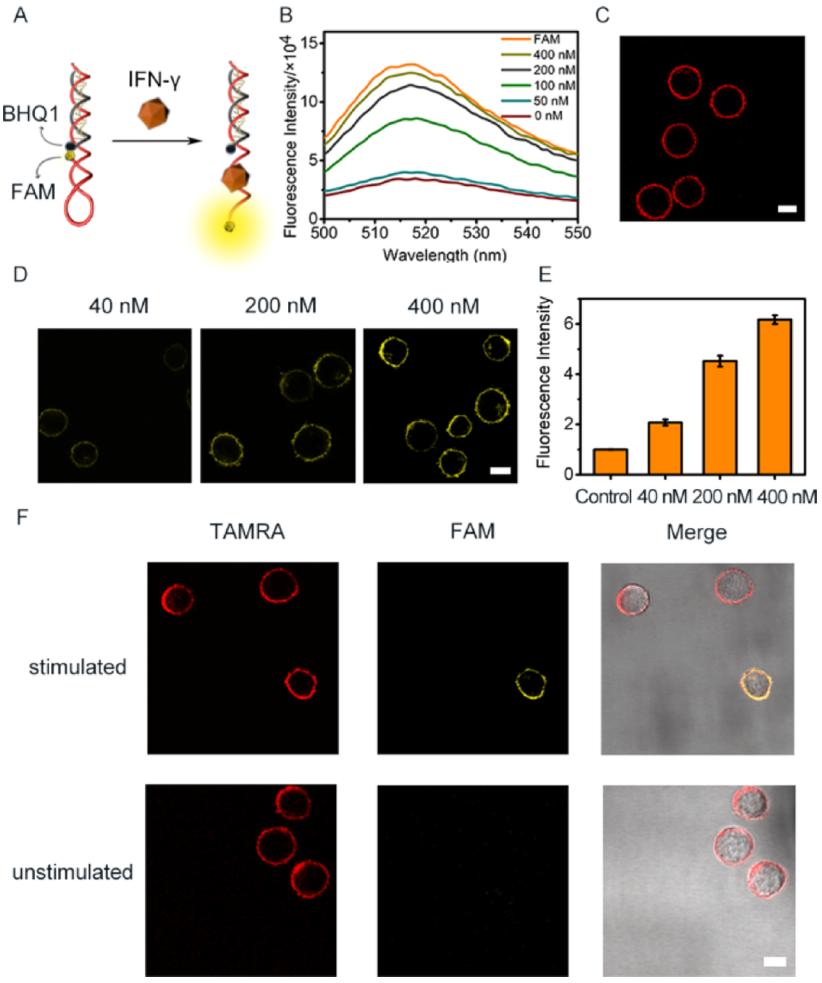

Figure 3. Monitoring cytokine IFN-γ secretion at the single-cell level. (A) Schematic diagram of the aptamer (IFN-γ) recognizing IFN-γ. (B) Fluorescence spectra of aptamer (IFN-γ) in response to various concentrations of IFN-γ from 0 to 400 nM. FAM indicates aptamer (IFN-γ)-FAM without BHQ1 modification. (C) Confocal microscopic images of DNA-copolymer nanocage-encapsulated U937 cells. Aptamer (IFN-γ)-TAMRA was used in the DNA-copolymer nanocage. (D) Confocal microscopic images and (E) corresponding FAM fluorescence recovery intensity of DNA-copolymer nanocage-encapsulated U937 cells in response to various concentrations of spiked IFN-γ. The error bars in (E) indicate means ± S.D. (n = 3). (F) Confocal microscopic images of DNA-copolymer-nanocage-encapsulated Jurkat cells with and without PMA and ionomycin stimulation. The scale bars in (C,D,F) are all 10 μm.

barely showed intracellular TAMRA fluorescence during the incubation period (Figure S14A), indicating little probe internalization. In contrast, cholesteryl-aptamer (IFN-γ)-TAMRA, which was functionalized with cholesteryl instead of acrydite, demonstrated a large degree of probe internalization during the incubation period with a high level of intracellular TAMRA fluorescence (Figure S14B). The solid assembly of the aptamer (IFN-γ) in the DNA-copolymer nanocage provided a stable sensing platform on the cell membrane, which confined the secreted cytokine locally around the secreting cell. The avoidance of sensing probe internalization also affected cell functions and physiological processes less. These would facilitate subsequent real-time cytokine secretion monitoring.

To monitor IFN-γ secretion in real time, the Jurkat cell was chosen as the model cell and assembled with the DNA-copolymer nanocage. S-DNA-copolymer-TAMRA$_{DNA3}$ was used in the DNA-copolymer nanocage to indicate its location. Jurkat cells were stimulated with PMA and ionomycin for cytokine IFN-γ secretion. All the cells demonstrated evenly distributed TAMRA fluorescence on the cell membrane (Figure 3F), indicating the successful construction of the DNA-copolymer nanocage. After 20 min stimulation, some cells demonstrated FAM fluorescence recovery (Figure 3F, stimulated), indicating the capability of the DNA-copolymer nanocage in IFN-γ secretion monitoring. FAM fluorescence was not observed from unstimulated cells (Figure 3F, unstimulated). Different from the situation for externally added recombinant IFN-γ, which showed similar FAM fluorescence intensity from different U937 cells in response to the same concentration of recombinant IFN-γ (Figure 3D), the cell-secreted IFN-γ resulted in different levels of FAM fluorescence recoveries on the cell membrane for different Jurkat cells. Some cells showed a large degree of FAM fluorescence recovery, while some cells barely showed FAM fluorescence recovery (Figure 3F, stimulated). The cell behavior heterogeneity in IFN-γ secretion upon stimulation was also confirmed by the flow cytometry assay, which showed only 14.9% of cells secreting IFN-γ (Figure S15). These results confirmed the capability of DNA-copolymer nanocages for monitoring cytokine secretion at the single-cell level, which confirmed the feasibility of screening cells according to their

https://doi.org/10.1021/acs.analchem.2c02763
Anal. Chem. 2022, 94, 13205−13214

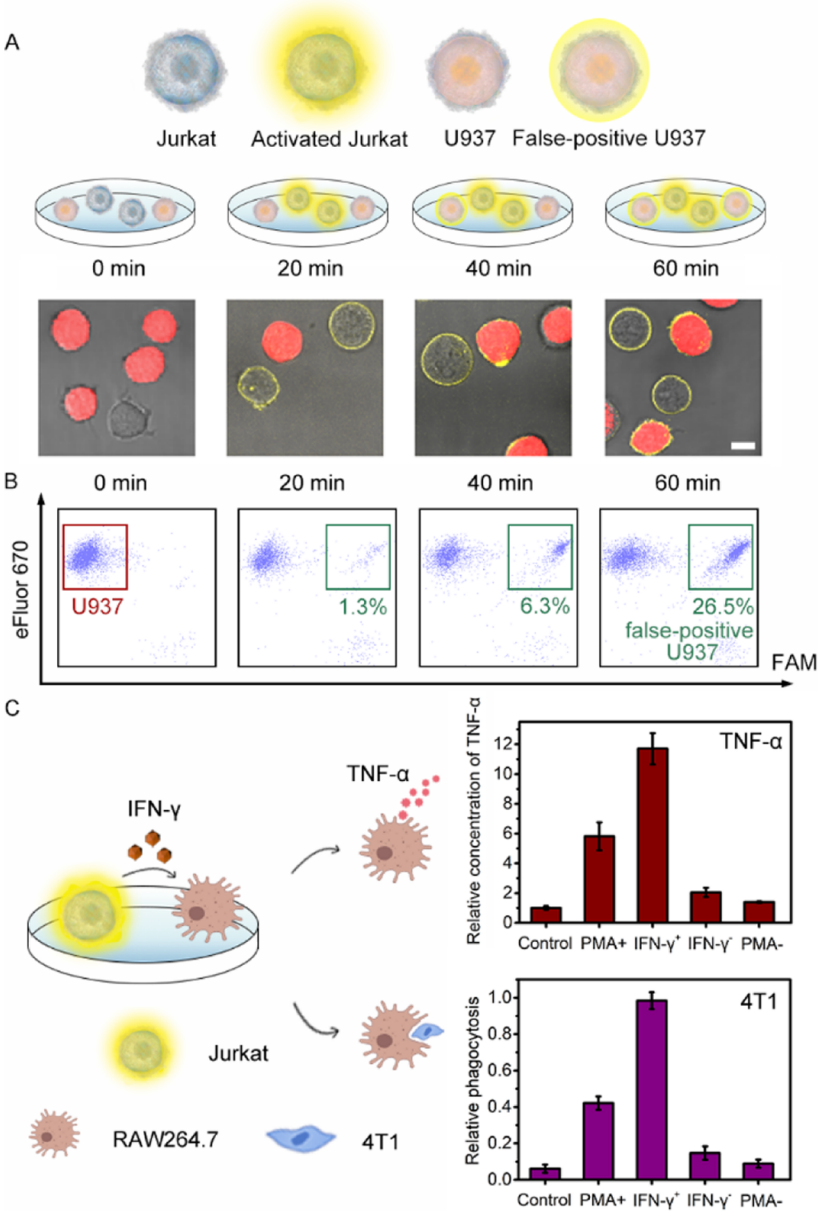

Figure 4. Jurkat cell activity selection and improved downstream cell activation. (A) Schematic illustration and confocal microscopic images and (B) flow cytometry assay of cocultured DNA-copolymer-encapsulated U937 cells (eFluor 670 pretreated) and DNA-copolymer-encapsulated Jurkat cells at different times after PMA and ionomycin stimulation. The scale bar in (A) is 10 μm. (C) Verification of RAW264.7 cell activation via TNF-α secretion (top, TNF-α) and phagocytosis of 4T1 cells (bottom, 4T1). RAW264.7 cells were cocultured with IFN-γ^+ Jurkat cells (IFN-γ^+), IFN-γ^- Jurkat cells (IFN-γ^-), stimulated but unselected Jurkat cells (PMA+), and unstimulated Jurkat cells (PMA−). Control indicates RAW264.7 cells that were not cocultured with Jurkat cells. The error bars indicate means ± S.D. (n = 3).

immune response heterogeneity. To verify the contribution of the DNA-copolymer nanocage on preventing cytokine diffusion between different cells, both IFN-γ secreting Jurkat cells and IFN-γ not secreting U937 cells were encapsulated with the DNA-copolymer nanocage or only D-DNA-copolymer, respectively. FAM fluorescence recovery on U937 cells indicated diffusion of IFN-γ among different cells. There was only 1.3% FAM fluorescence recovery from U937 cells equipped with the DNA-copolymer nanocage and 24.1% from U937 cells equipped with the D-DNA-copolymer (Figure S16), which would benefit IFN-γ^+ cell sorting. The as-constructed DNA-copolymer nanocage demonstrated good biocompatibility and showed little effect on cell viability measured by the live/dead dual staining kit and CCK-8 kit (Figure S17A,B) and cytokine secretion capability (Figure S17C) compared with unengineered Jurkat cells.

Cell Activity Selection with Enhanced Performance in Cell−Cell Interaction. Preventing the intercellular diffusion of secreted cytokine during the detection period is important to distinguish cell immune response heterogeneity. The DNA-copolymer nanocage constructed on the cell membrane could confine IFN-γ locally around the secreting cell during the detection period. To verify the confinement effect of the DNA-copolymer nanocage, U937 cells, which do not secret IFN-γ, were pretreated with cytoplasm dye eFluor 670 (red) as the indicator and constructed with the DNA-copolymer nanocage. The as-prepared U937 cells were cocultured with the DNA-copolymer nanocage functionalized Jurkat cells and stimulated

https://doi.org/10.1021/acs.analchem.2c02763
Anal. Chem. 2022, 94, 13205−13214

with PMA and ionomycin for Jurkat cells to secrete IFN-γ. At 20 min after stimulation, FAM fluorescence was only observed on Jurkat cells, indicating the satisfactory prevention of intercellular IFN-γ diffusion. FAM fluorescence recovery started to show up on some U937 cells located close to Jurkat cells at 40 min, indicating the diffusion of secreted IFN-γ to nearby cells. At 60 min after stimulation, the secreted IFN-γ spread to more U937 cells (Figure 4A). Compared with the dense DNA constructions on the cell membrane,[28] the assembly of DNA-copolymer nanocage not only isolated individual cells but also provided space for the easy migration of secreted IFN-γ locally around the secreting cell, which guaranteed efficient sensing of the single-cell immune response. Encapsulation with the DNA-copolymer nanocage generated about 20 min as the detection window after cell stimulation, which allowed sufficient recovery of FAM fluorescence from secreting cells and eliminated the generation of a "false-positive" signal at adjacent cells. The flow cytometry assay results further confirmed 20 min as the detection window for IFN-γ secretion on DNA-copolymer nanocage-encapsulated cells. There was only 1.3% of cocultured U937 cells that demonstrated "false-positive" FAM fluorescence recovery at 20 min due to IFN-γ diffusion from adjacent cells. The percentage of "false-positive" U937 cells gradually increased with time and reached 26.5% at 60 min (Figure 4B). Selecting active T cells with higher IFN-γ secretion capability and removing inactive ones could improve cell therapeutic effects. Jurkat cells were selected via FACS based on FAM fluorescence recovery that indicated IFN-γ secretion capability. Active Jurkat cells were characterized as IFN-γ secretion above 100 pg/mL;[10] thus, Jurkat cells showed that the corresponding FAM fluorescence recovery was defined as IFN-γ^+ Jurkat cells here and were retained after FACS. Jurkat cells with lower FAM fluorescence recovery were defined as IFN-γ^- Jurkat cells and were discarded after FACS. Macrophage RAW264.7 was chosen to establish a cell−cell communication model to verify the contribution of cell selection to Jurkat cell immune response. The sorted Jurkat cells were irradiated with UV light to detach the DNA-copolymer nanocage and cocultured with RAW264.7 cells. Cytokine tumor necrosis factor-α (TNF-α) secretion from RAW264.7 cells was measured by ELISA after 24 h. RAW264.7 cells cocultured with IFN-γ^+ Jurkat cells showed the highest secretion level of TNF-α (Figure 4C, TNF-α, IFN-γ^+), 5.8-fold compared with those incubated with IFN-γ^- Jurkat cells (Figure 4C, TNF-α, IFN-γ^-) and 1.9-fold compared with those incubated with stimulated but unselected Jurkat cells (Figure 4C, TNF-α, PMA+). RAW264.7 cells cocultured with IFN-γ^- Jurkat cells showed similar secretion levels of TNF-α compared with those incubated with unstimulated Jurkat cells (Figure 4C, TNF-α, PMA-) and those without coculturing (Figure 4C, TNF-α, control). This result indicated that IFN-γ^- Jurkat cells barely contributed to RAW264.7 cell activation. In addition, the above treated RAW264.7 cells were collected, respectively, and cocultured with 4T1 cells, and the phagocytosis capability of RAW264.7 cells was evaluated by measuring the viability of 4T1 cells. RAW264.7 cells that were cocultured with IFN-γ^+ Jurkat cells showed that 6.7-fold 4T1 cells digest (Figure 4C, 4T1, IFN-γ^+) compared with those cocultured with IFN-γ^- Jurkat cells (Figure 4C, 4T1, IFN-γ^-) and 2.3-fold compared with those cocultured with unselected Jurkat cells (Figure 4C, 4T1, PMA+). RAW264.7 cells cocultured with IFN-γ^- Jurkat cells showed a similar 4T1 digest capability compared with those cocultured with unstimulated Jurkat cells (Figure 4C, 4T1, PMA-) and those not cocultured with Jurkat cells (Figure 4C, 4T1, control). These results demonstrated that IFN-γ secretion-based cell screening and selection could improve Jurkat cell immune response and promote downstream cell activation in immunotherapy.

The cell membrane-assembled DNA-copolymer nanocage was further applied to CAR-T cell activity evaluation and cell screening. CD19 CAR-T cells were activated by preincubating with Raji cells (CD19$^+$) and assembled with the DNA-copolymer on the cell membrane. Raji cells were pretreated with the cytoplasm dye eFluor 670 (red) as the indicator for distinguishing them (Figure 5A, DNA-copolymer construction). The DNA-copolymer nanocage was labeled with TAMRA to indicate its location, which demonstrated obvious and evenly distributed TAMRA fluorescence on both the CAR-T cell membrane and Raji cell membrane, indicating the successful construction of the DNA-copolymer nanocage on the cell membrane (Figure S18).

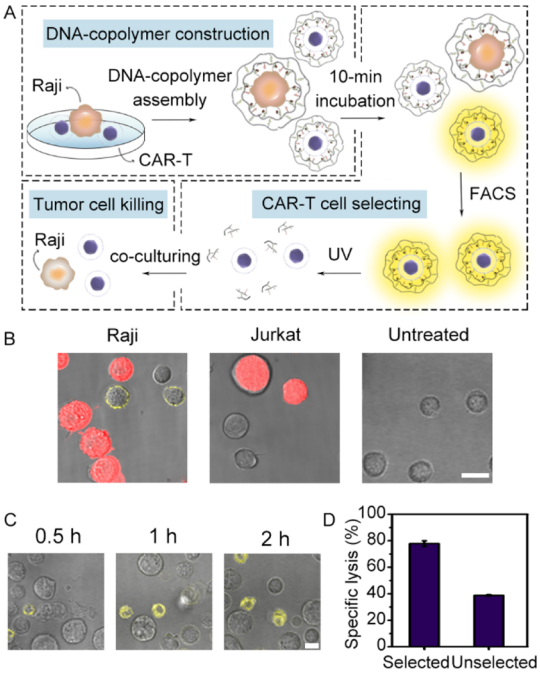

Figure 5. CD 19 CAR-T cell activity selection and enhanced tumor cell killing. (A) Schematic illustration of CAR-T cell activity screening via the membrane-detachable DNA-copolymer and verification of tumor cell killing capability of selected CAR-T cells. Confocal microscopic images of (B) CD19 CAR-T cells treated with Raji cells (Raji), Jurkat cells (Jurkat), and CD19 CAR-T cells not cocultured with any other cell line (untreated), and (C) CD19 CAR-T cells and Raji cells with different coculturing times from 0.5 to 2 h before the construction of the DNA-copolymer nanocage. The scale bar is 10 μm. (D) Specific lysis of Raji cells after coculturing with selected CD19 CAR-T cells (selected) and *ex vivo*-expanded CD19 CAR-T cell population (unselected). The error bars indicate means ± S.D. (n = 3).

After continuously incubating for 10 min, clear FAM fluorescence recovery was observed on some CAR-T cells, indicating good IFN-γ secretion capability (Figure 5B, Raji). On the contrary, FAM fluorescence recovery was barely observed on CAR-T cells that were incubated with Jurkat cells (CD19$^-$) (Figure 5B, Jurkat) or CAR-T cells that were not

https://doi.org/10.1021/acs.analchem.2c02763
Anal. Chem. 2022, 94, 13205−13214

cocultured with other cell lines (Figure 5B, untreated). "False-positive" FAM fluorescence recovery was barely observed from the cocultured Raji cell membrane (Figure 5B, Raji), indicating the satisfactory local confinement of IFN-γ around secreting cells and the successful avoidance of nearby cell interference during the detection period. To further demonstrate the feasibility of selecting active CAR-T cells via the cell membrane-assembled DNA-copolymer nanocage, CD19 CAR-T cells were cocultured with Raji cells at different times to generate different activation levels. Those CAR-T cells with longer coculturing time demonstrated a higher level of activation with a larger number of FAM fluorescent cells (Figure 5C). IFN-γ secretion was also quantified using an ELISA kit from the supernatant of CD19 CAR-T cells and Raji cell cocultures, which demonstrated a similar tendency of increased IFN-γ secretion with prolonged coculture time (Figure S19).

The active CAR-T cells with FAM fluorescence recovery were selected via FACS and exposed to 5 min UV light to detach the DNA-copolymer nanocage (Figure 5A, CAR-T cell selection). To evaluate the immune response of the selected CAR-T cells, they were subsequently cocultured with Raji cells. The tumor cell killing capability of CAR-T cells was determined by measuring the viability of Raji cells using a CCK-8 kit (Figure 5A, Tumor cell killing). By coculturing with sorted CAR-T cells, Raji cells showed a 2.0-fold lysis percentage compared with those incubated with unsorted CAR-T cells (Figure 5D). These results suggested that IFN-γ secretion-based cell sorting could boost its immune response and improve T-cell killing capability, which may have promising applications in adoptive cell immunotherapy.

CONCLUSIONS

A detachable DNA-copolymer nanocage was constructed on the T-cell membrane in this work to screen cytokine IFN-γ secretion from a single cell in real time. It confined the secreted IFN-γ locally around secreting cells and eliminated interference from nearby cell secretion during the detection period. Therefore, single T-cell activity heterogeneity was discriminated by measuring FAM fluorescence recovery from the DNA-copolymer nanocage in response to IFN-γ secretion. The active T cells were correspondingly selected via FACS and exposed for 5 min to UV light to detach the DNA-copolymer nanocage, which demonstrated enhanced capabilities for downstream cell activation and tumor cell killing. The detachable DNA-copolymer nanocage on the cell membrane achieved successful application in cell activity screening and selection for Jurkat cells and CD19 CAR-T cells, indicating potential application in adaptive cell immunotherapy.y.

ASSOCIATED CONTENT

Supporting Information

The Supporting Information is available free of charge at https://pubs.acs.org/doi/10.1021/acs.analchem.2c02763.

Materials and reagents, apparatus, gel electrophoresis analysis, *in vitro* verification of DNA-copolymer hybridization, *in vitro* detection of IFN-γ, biocompatibility assay, and feasibility verification of cell screening (PDF)

AUTHOR INFORMATION

Corresponding Authors

Peipei Xu − *Department of Hematology, Nanjing Drum Tower Hospital, School of Medicine, Nanjing University, Nanjing 210093, China*; Email: xu_peipei0618@163.com

Ying Liu − *State Key Laboratory of Analytical Chemistry for Life Science, School of Chemistry and Chemical Engineering and Chemistry and Biomedicine Innovation Center, Nanjing University, Nanjing 210023, China*; orcid.org/0000-0001-5718-7804; Phone: +86-(0)25-89681918; Email: yingliu@nju.edu.cn; Fax: /Phone

Authors

Yanyun Fang − *State Key Laboratory of Analytical Chemistry for Life Science, School of Chemistry and Chemical Engineering, Nanjing University, Nanjing 210023, China*

Yawei Yan − *State Key Laboratory of Analytical Chemistry for Life Science, School of Chemistry and Chemical Engineering, Nanjing University, Nanjing 210023, China*

Shiyi Bi − *State Key Laboratory of Analytical Chemistry for Life Science, School of Chemistry and Chemical Engineering, Nanjing University, Nanjing 210023, China*

Yingfei Wang − *State Key Laboratory of Analytical Chemistry for Life Science, School of Chemistry and Chemical Engineering, Nanjing University, Nanjing 210023, China*

Yue Chen − *Department of Hematology, Nanjing Drum Tower Hospital, School of Medicine, Nanjing University, Nanjing 210093, China*

Huangxian Ju − *State Key Laboratory of Analytical Chemistry for Life Science, School of Chemistry and Chemical Engineering, Nanjing University, Nanjing 210023, China*; orcid.org/0000-0002-6741-5302

Complete contact information is available at: https://pubs.acs.org/10.1021/acs.analchem.2c02763

Notes

The authors declare no competing financial interest.

ACKNOWLEDGMENTS

We thank Dr. Guang Hu (Nanjing Biotech and Pharmaceutical Valley, China) for his valuable suggestion. We gratefully acknowledge the National Natural Science Foundation of China (22022405, 21974064, and 82170224), Natural Science Foundation of Jiangsu Province for distinguished Young Scholars (BK20200010), specially appointed Professor Foundation of Jiangsu Province, and Program for Innovative Talents and Entrepreneurs of Jiangsu Province.

REFERENCES

(1) Rosenberg, S. A.; Restifo, N. P. *Science* **2015**, *348*, 62−68.
(2) Zhang, D.; Zheng, Y.; Lin, Z.; Liu, X.; Li, J.; Yang, H.; Tan, W. *Angew. Chem., Int. Ed.* **2020**, *59*, 12022−12028.
(3) Qin, S.; Melucci, A. D.; Chacon, A. C.; Prieto, P. A. *Cells* **2021**, *10*, 808.
(4) Rosenberg, S. A.; Packard, B. S.; Aebersold, P. M.; Solomon, D.; Topalian, S. L.; Toy, S. T.; Simon, P.; Lotze, M. T.; Yang, J. C.; Seipp, C. A.; Simpson, C.; Carter, C.; Bock, S.; Schwartzentruber, D.; Wei, J. P.; White, D. E. *N. Engl. J. Med.* **1988**, *319*, 1676−1680.
(5) Liu, Z.; Li, J. P.; Chen, M.; Wu, M.; Shi, Y.; Li, W.; Teijaro, J. R.; Wu, P. *Cell* **2020**, *183*, 1117−1133.
(6) Schumacher, T. N.; Schreiber, R. D. *Science* **2015**, *348*, 69−74.
(7) Chen, Z.; Chen, J. J.; Fan, R. *Annu. Rev. Anal. Chem.* **2019**, *12*, 431−449.
(8) Paul, W. E.; Seder, R. A. *Cell* **1994**, *76*, 241−251.

(9) Sachdeva, N.; Asthana, D. *Front. Biosci.* **2007**, *12*, 4682−4695.
(10) Dudley, M. E.; Wunderlich, J. R.; Shelton, T. E.; Even, J.; Rosenberg, S. A. *J. Immunother.* **2003**, *26*, 332−342.
(11) Yu, L.; Feng, R.; Zhu, L.; Hao, Q.; Chu, J.; Gu, Y.; Luo, Y.; Zhang, Z.; Chen, G.; Chen, H. *Sci. Adv.* **2020**, *6*, No. eabb6595.
(12) Bahmani, B.; Gong, H.; Luk, B. T.; et al. *Nat. Commun.* **2021**, *12*, 1999.
(13) Kongsuphol, P.; Lee, G. C. F.; Arya, S. K.; Chiam, S. Y.; Park, M. K. *Sens. Actuators, B* **2017**, *244*, 823−830.
(14) Krueger, A.; Stoll, T.; Shah, A. K.; Sinha, R.; Frazer, I. H.; Hill, M. M. *Anal. Chem.* **2020**, *92*, 3742−3750.
(15) Bucheli, O. T. M.; Sigvaldadóttir, I.; Eyer, K. *Eur. J. Immunol.* **2021**, *51*, 1334−1347.
(16) Zhou, Y.; Shao, N.; Bessa de Castro, R. B.; Zhang, P.; Ma, Y.; Liu, X.; Huang, F.; Wang, R.; Qin, L. *Cell Rep.* **2020**, *31*, 107574.
(17) Antona, S.; Abele, T.; Jahnke, K.; Dreher, Y.; Göpfrich, K.; Platzman, I.; Spatz, J. P. *Adv. Funct. Mater.* **2020**, *30*, 2003479.
(18) Qiu, L.; Wimmers, F.; Weiden, J.; Heus, H. A.; Tel, J.; Figdor, C. G. *Chem. Commun.* **2017**, *53*, 8066−8069.
(19) Jia, H.; Zhu, Y.; Duan, Q.; Wu, F. *Chem. Soc. Rev.* **2021**, *50*, 6240−6277.
(20) Zhao, W.; Schafer, S.; Choi, J.; Yamanaka, Y. J.; Lombardi, M. L.; Bose, S.; Carlson, A. L.; Phillips, J. A.; Teo, W.; Droujinine, I. A.; Cui, C. H.; Jain, R. K.; Lammerding, J.; Love, J. C.; Lin, C. P.; Sarkar, D.; Karnik, R.; Karp, J. M. *Nat. Nanotechnol.* **2011**, *6*, 524−531.
(21) Liu, G.; Bursill, C.; Cartland, S. P.; Anwer, A. G.; Parker, L. M.; Zhang, K.; Feng, S.; He, M.; Inglis, D. W.; Kavurma, M. M.; Hutchinson, M. R.; Goldys, E. M. *iScience* **2019**, *20*, 137−147.
(22) Kida, A.; Iijima, M.; Niimi, T.; Maturana, A. D.; Yoshimoto, N.; Kuroda, S. *Anal. Chem.* **2013**, *85*, 1753−1759.
(23) Pavillon, N.; Hobro, A. J.; Akira, S.; Smith, N. I. *Proc. Natl. Acad. Sci. U.S.A.* **2018**, *115*, E2676−E2685.
(24) Qiu, L.; Zhang, T.; Jiang, J.; Wu, C.; Zhu, G.; You, M.; Chen, X.; Zhang, L.; Cui, C.; Yu, R.; Tan, W. *J. Am. Chem. Soc.* **2014**, *136*, 13090−13093.
(25) Qian, R.; Zhou, Z.; Guo, W.; Wu, Y.; Yang, Z.; Lu, Y. *J. Am. Chem. Soc.* **2021**, *143*, 5737−5744.
(26) Liu, Y.; Liu, Y.; Matharu, Z.; Rahimian, A.; Revzin, A. *Biosens. Bioelectron.* **2015**, *64*, 43−50.
(27) Shin, D.-S.; Matharu, Z.; You, J.; Siltanen, C.; Vu, T.; Raghunathan, V. K.; Stybayeva, G.; Hill, A. E.; Revzin, A. *Adv. Healthcare Mater.* **2016**, *5*, 659−664.
(28) Gao, T.; Chen, T.; Feng, C.; He, X.; Mu, C.; Anzai, J.; Li, G. *Nat. Commun.* **2019**, *10*, 2946.

https://doi.org/10.1021/acs.analchem.2c02763
Anal. Chem. 2022, 94, 13205−13214